# Theoretical deposition of carcinogenic particle aggregates in the upper respiratory tract

**Robert Sturm**

Brunnleitenweg 41, 5061 Elsbethen, Salzburg, Austria

*Corresponding to:* Dr. Robert Sturm. Brunnleitenweg 41, 5061 Elsbethen, Salzburg, Austria. Email: Robert.Sturm@stud.sbg.ac.at.

**Background:** Numerous particles suspended in the atmosphere are composed of smaller particular components that form aggregates with highly irregular shape. Such aggregates, among which dusts and soot are the most prominent examples, may be taken up into the respiratory tract and, in the worst case, initiate a malignant transformation of lung cells.

**Methods:** Particle aggregates were theoretically modelled by using small spheres with equal diameters (1 nm) and arranging them randomly. This procedure resulted in the generation of various aggregate shapes (chain-like, loose, compact), for which essential parameters such as dynamic shape factors, $\chi$, and aerodynamic diameters, $d_{ae}$, were computed. Deposition of aggregates consisting of 10, 50, 100, and 1,000 nano-spheres was simulated for the uppermost parts of the human respiratory system (extrathoracic region and airway generation 0 to 4), thereby distinguishing between sitting and light-work breathing as well as between nasal and oral inhalation.

**Results:** Based upon the modelling results, aggregate deposition in the human respiratory system can be described as a function of (I) aerodynamic diameter; (II) inhaled particle position within the airway system; and (III) breathing conditions. Therefore, highest deposition values were obtained for nano-scale aggregates (<10 nm), whereas larger aggregates exhibited slightly to significantly reduced deposition probabilities. Extrathoracic regions and uppermost bronchi (generations 0 to 1) were marked by most effective particle capture. Any increase of inhaled air volumes and reduction of breathing times resulted in an enhancement of deposition probabilities of larger particles.

**Conclusions:** Based on the results derived from this study it may be concluded that small particle aggregates are accumulated in the uppermost compartments of the human respiratory tract, where they may unfold their unwholesome potential. In the case of carcinogenic particles being stored in epithelial cells for a longer time span, malignant transformations starting with the formation of cancerous cells and ending with the growth of a tumour have to be assumed.

**Key Words:** Lung deposition; ultrafine particles; deposition model; lung; particle aggregates; deposition; lung; Monte-Carlo model

Submitted Jun 29, 2013. Accepted for publication Jul 19, 2013.

doi: 10.3978/j.issn.2305-5839.2013.07.06

**Scan to your mobile device or view this article at:** http://www.atmjournal.org/article/view/2385/3251

## Introduction

Particles being suspended in the ambient air may be regarded as serious health hazards when they are taken up via the respiratory tract. Additionally, they may have remarkable effects on the climatic cycle, atmospheric transparency, and environmental deposition of acidic and toxic substances. Apart from these hygienic and environmental aspects, aerosol particles have also found their applications in numerous industrial processes. Independent of the site, where such particular matter is formed, physical properties of airborne particles are chiefly controlled by particle size and shape. This is also the reason,

why many methods of aerosol concentration measurement are founded upon the determination of particle diameter classes (1-4).

Smoke and soot represent aerosol particles that result from combustion or thermal decomposition processes. Besides their classification as so-called ultrafine particles, i.e., particles with diameters less than 100 nm, they are commonly characterized by a highly irregular shape, regardless of origin and chemical composition. Irregularly shaped particular substances substances are frequently composed of high numbers of primary particles that form a so-called aggregate (5,6). In the past, theoretical visualization of such aggregates was significantly simplified by defining the primary components as small spheres or spherules that are combined in a stochastic or even chaotic manner (6-8). Measurements of atmospheric aerosols provide clear evidence that ultrafine particle aggregates are practically always detected in the ambient air volume (9), wherefore they have considerable influences on human health.

Recent mathematical models describing particle aggregate geometry are based upon fractal geometry, being able for the simulation of highly chaotic and nearly realistic shapes (10,11). Especially shapes of soot particles emitted from diesel engines are approximated by these models, because they have excited public interest during the past decades due to their contribution to the burden of pulmonary and cardiovascular diseases (12,13). Theoretical approaches of aggregate geometry and related behaviour of such particle complexes in the continuum regime and slip flow regime date back to the 1970s (6-8) and 1980s (5,14). According to Kasper (5) aggregate geometry may be subdivided into two main categories: the first category includes clusters that can be treated like a porous sphere, whilst the second category comprises chains corresponding in their behaviour to prolate bodies. Mathematical approaches conducted more currently have subjected Kasper's classification of aerosol aggregates to a further significant refinement. Basically aggregates are supposed to consist of small, equally sized spheres that either form clusters without any voids, compact aggregates with internal voids or, most likely, loose aggregates with internal voids (15,16). Each of these three categories is characterized by individual diameters, volumes and dynamic shape factors. Microscopic studies on soot particles deposited in the lungs and consequently captured in the bronchial and alveolar parenchyma of laboratory animals (17,18) provide clear evidence that cluster geometry may be most appropriately simulated by loose and compact aggregates of spherules with internal voids. Due to their deposition in the lungs and subsequent capture in bronchial and alveolar tissues soot particles have excited increased medical interest. Within these specific tissues they may be stored for years and partly act as triggers for malignant transformations. Microscopic images additionally show that soot clusters may be most reliably approximated by loose or compact aggregates of small spheres, whereby these aggregates are marked by internal voids.

The objective presented here is two-fold: first, deposition scenarios of particle aggregates with variable shapes are simulated for the extrathoracic region (i.e., the nasal/oral air passages and nasopharynx/oropharynx) as well as the proximal part (airway generations 0 to 4) of the tracheobronchial tree of the human respiratory tract. Second, possible effects of aggregate deposition on the formation of lung cancer are discussed.

## Methods

### *Theoretical generation of particle aggregates and related dynamic shape factors*

Particle aggregates were generated according to the mathematical algorithm currently introduced by Sturm (19). This approach allows the use of spherical components with various diameters as well as the variation of the number of spheres used for the construction of the aggregates. Shapes of the aggregates are founded upon the random number concept, resulting in compact, loose or even ramified aggregate geometries.

The diameter of an aggregate, $d_{es}$, basically corresponds to the diameter of a sphere wrapping around the multi-component particle (19). Estimation of the dynamic shape factor, $\chi$, is conducted according to the equation [1] (5):

$$\chi = \frac{d_{es}}{d_{ve}} \quad [1]$$

with $d_{ve}$ denoting the diameter of a sphere with exactly the same volume as the aggregate of interest (volume equivalent diameter). The computation of $d_{ve}$ is simply realized by the equation [2]:

$$d_{ve} = \sqrt[3]{\sum_{i=1}^{n} d_i^3} \quad [2]$$

where $n$ represents the number of spherical components of the aggregate, whilst $d_i$ corresponds to the diameter of spherical component $i$. Finally, the aerodynamic diameter

 

of a given aggregate is derived from the widely applied equation [3] (5-8,19):

$$d_{ae} = d_{ve} \cdot \sqrt{\frac{1}{\chi} \cdot \frac{\rho_p}{\rho_0} \cdot \frac{C(d_{ve})}{C(d_{ae})}} \quad [3]$$

In the expression noted above $\rho_p$ and $\rho_0$ denote the mean density of the particle aggregate of interest as well as unit density (1 g·cm$^{-3}$), respectively, whereas C($d_{ve}$) and C($d_{ae}$) correspond to the Cunningham slip correction factors related to $d_{ve}$ and $d_{ae}$. Calculation of particle slip correction may be carried out according to the general equation [4]:

$$C(d) = 1 + \frac{2\lambda}{d} \cdot \left[a + b \cdot \exp\left(\frac{c}{2\lambda/d}\right)\right] \quad [4]$$

where λ represents the mean free molecular path length of air (0.066 μm at 20 ℃) and d the respective particle diameter ($d_{ve}$ or $d_{ae}$). The empirical coefficients a, b, and c are commonly provided by reviews dealing with that topic (5-8). The formula of the Cunningham slip correction factor may be applied to the continuum regime with Knudsen number, $K_n$, adopting values <<1 as well as to the free-molecular regime with $K_n$ adopting values >>1. Within the continuum regime particles with diameters >0.5 μm are usually used for calculations, resulting in Cunningham slip correction factors that increasingly tend to take the value 1 and, therefore, can be omitted from equation [3].

### *Computation of aggregate deposition in the human respiratory tract*

Deposition of particle aggregates in the upper airways of the respiratory system was simulated by using (I) the aerodynamic diameter concept described above and (II) the stochastic particle transport and deposition model introduced in numerous preceding publications (20-24). According to the stochastic approach to particle transport and deposition transport trajectories of single aggregates through the tracheobronchial tree are selected on the basis of the random number concept, whereby at each airway bifurcation the further progress of an inhaled particle is computed separately. The decision of the particle to enter either the left or the right daughter airway partly depends on the distribution of inhaled air volume between the two daughter tubes.

Lung structure was systematically generated by random selection of geometric determinants (airway diameter, airway length, bifurcation angle, gravitation angle) from predefined lung generation-specific probability density functions (25), which are based on morphometric data sets of the human respiratory tract (26,27).

Aggregate deposition in the thoracic airways and alveoli of the respiratory system was simulated by application of empirical formulae for the four main deposition forces, namely Brownian diffusion, inertial impaction, interception, and gravitational settling (20,28). The combined effect of these deposition forces on single particles taken up during inhalation was computed with the help of mathematical equations expressing the fraction of each deposition mechanism as function of the aerodynamic diameter. For a statistical evaluation of such theoretically computed deposition scenarios, high numbers (usually 10,000) of randomly constructed particle trajectories through the airway structure were produced and submitted to statistical standard procedures. Additional optimization of these computations took place by application of the statistical weight method which allows each particle to perform multiple deposition events (20,29). Thereby, the probability of each deposition event was weighted against related deposition events that had taken place in preceding airway generations. Particle deposition was finally expressed as function of lung region (bronchial *vs.* alveolar) and lung generation-specific deposition site.

Concerning extrathoracic aggregate deposition, i.e., deposition of non-spherical particles in the oral, nasal, and pharyngeal air passages, approximations based on mathematical regression procedures and expressing deposition fraction as function of diffusion coefficient and flow rate were used. For the oral airways illustrated in *Figure 1*, the following deposition equation [5] for the diffusion regime was applied (30-33):

$$D_{oral} = 1 - \exp(-20.4 + 4.1 \cdot D^{0.66\pm0.04} \cdot Q^{-0.31\pm0.07}) \quad [5]$$

For the nasal air passage, being marked by significantly higher complexity in structure than the oral airways (*Figures 1*,*2*), deposition may be computed with the following equation [6] (31):

$$D_{nasal} = 1 - \exp(-16.6 + 4.5 \cdot D^{0.50\pm0.02} \cdot Q^{-0.28\pm0.09}) \quad [6]$$

$D_{oral}$ and $D_{nasal}$ denote oral and nasal deposition fraction, respectively, whereas $Q$ denotes the flow rate (L·min$^{-1}$) and $D$ yields the diffusion coefficient which is commonly defined by the mathematical expression [7]

 

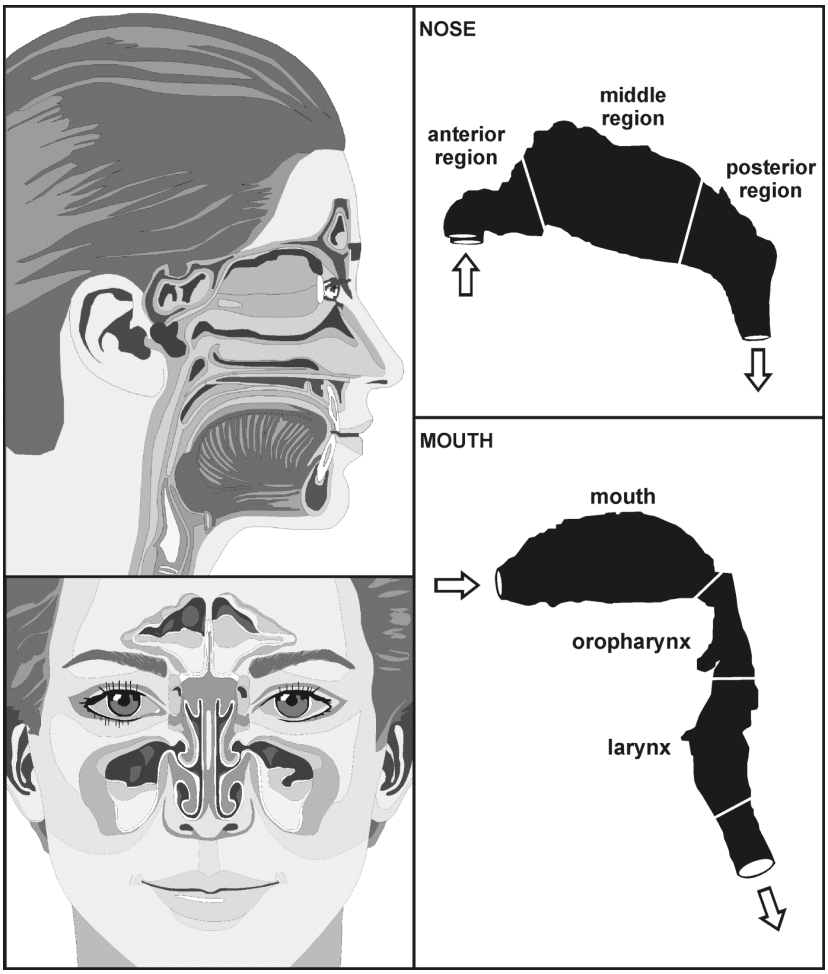


**Figure 1** Theoretical sketch illustrating the anatomy of oral and nasal pathways of the human respiratory tract (left) as well as geometric models standing behind the simulation of extrathoracic particle deposition (30,31)

$$D = \frac{2}{3} \cdot \frac{1}{n d_{ae}^2} \cdot \sqrt{\frac{k_B T}{\pi^3 m}} \quad [7]$$

with $n$ denoting the number of particles within a unit-volume (1 $m^3$), $d$ representing the aerodynamic particle diameter, $k_B$ being the Boltzmann constant ($J \cdot K^{-1}$), T being the temperature of the fluid, and m representing the molecule mass (kg).

## Modelling results

### *Construction of particle aggregates*

Particle aggregates were theoretically constructed in the way described above. For aggregate generation different numbers of equally sized spherical components were used: small aggregates were composed of 10 spheres, intermediately sized aggregates of 50 and 100 spheres, and large aggregates of 1,000 spheres, respectively. Shape of the theoretically computed aggregate particles was subject to high variation, ranging from chain-like structures to more compact structures with internal voids (*Figure 3*) and almost spherical structures with a rather massive appearance. Depending on the geometry of the aggregates high variations of $\chi$ and, as a consequence of that, of $d_{ae}$ could be modelled which are summarized in *Figure 4*. Therefore, aggregates consisting of only 10 spheres with equal size (diameter: 1 nm) show a $\chi$ ranging from 1.1 to 2.4 and a $d_{ae}$ varying between 1.39 and 2.04 nm. For aggregates being composed of 50 spheres $\chi$ and $d_{ae}$ are both subject to a significant increase, thereby taking values between 1.2 and 7.5 and values between 1.34 and 3.36 nm. This trend is further continued for aggregates

 

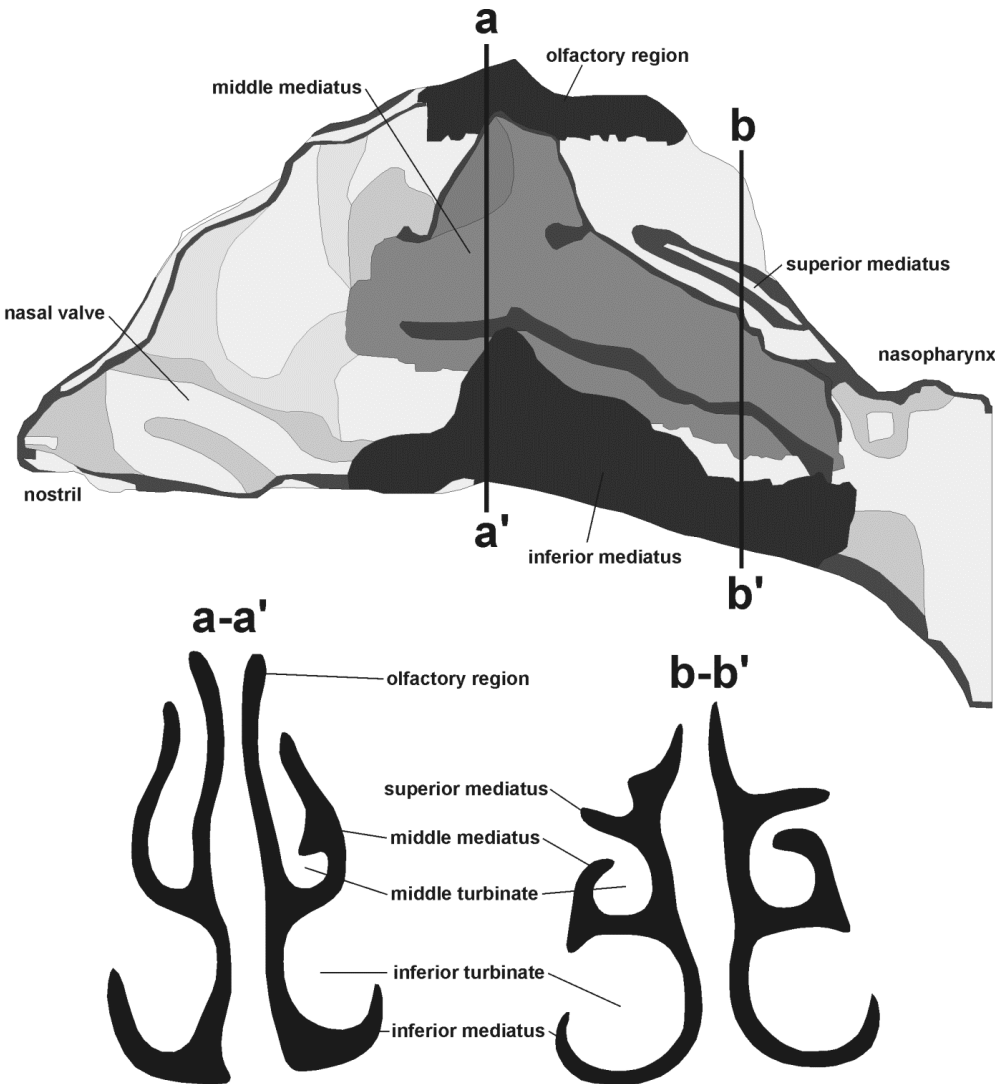


**Figure 2** Detailed anatomical model of the nasal pathway including respective wall roughness emanating from nasal conchae (30)

comprising 100 spheres ($\chi$: 1.6-12.3; $d_{ae}$: 1.32-3.66 nm). Finally, aggregates being constructed of 1,000 spheres vary in dynamic shape factor between 1.9 and 43.6, whilst the aerodynamic diameter commonly ranges from 1.51 to 7.25 nm (*Figure 4*). Based on these data aerodynamic diameter, $d_{ae}$, commonly varies between 1 and 8 nm.

### *Deposition of particle aggregates in specific airways of the upper respiratory tract*

Deposition computations were carried out by assuming (I) sitting breathing conditions (tidal volume: 750 mL, breathing cycle length: 4.2 s) and (II) light-work breathing conditions (tidal volume: 1,250 mL, breathing cycle

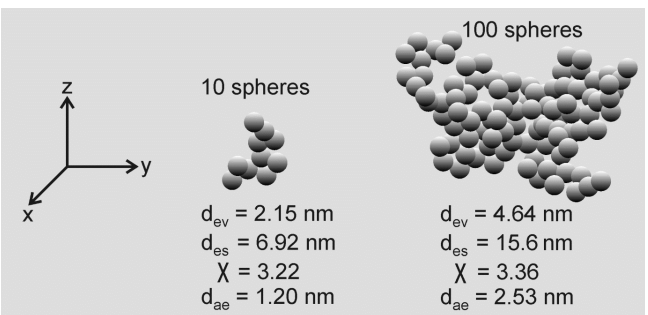


**Figure 3** Examples of particle aggregates consisting of 10 equally sized spheres (d =1 nm) and 100 equally sized spheres. Values for $d_{ev}$, $d_{es}$, $\chi$, and $d_{ae}$ were computed with the help of the theoretical model presented in this study

 

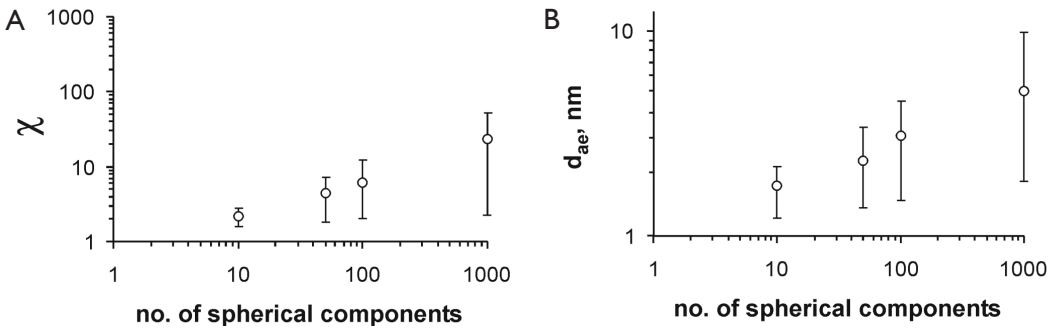


**Figure 4** Computation of essential geometric parameters (mean ± standard deviation) describing the size of multiple-sphere aggregates. Aggregates were assumed to consist of 10, 50, 100, and 1,000 equally sized spheres (d =1 nm). A. Dynamic shape factor ($\chi$); B. Aerodynamic diameter ($d_{ae}$)

length: 3 s). Concerning the sitting breathing scenarios, respective modelling results are summarized in *Figure 5*. In the graphs of *Figure 5* aggregate deposition in the extrathoracic compartment and airway generations 0 (trachea) to 4 is presented as a function of the aerodynamic particle diameter $d_{ae}$. Solid curves describe particle deposition after passage of the nasal pathway, whilst dashed curves describe particle deposition following inhalation through the oral pathway. In the extrathoracic region including oral/nasal cavities and oro-/nasopharynx (*Figure 5A*) highest deposition values may be attested for particle aggregates with $d_{ae}$ <10 nm (40-90%), whereas deposition efficiency of larger particles continuously declines with increasing size and finally reaches a minimum for $d_{ae}$ ≈0.5 µm (0.8-10.2%). For larger particles extrathoracic deposition is again subject to a steep increase, reaching another maximum at $d_{ae}$ =10 µm (85-98%). Deposition in the nasal airways is commonly higher than that in the oral airways, with deposition discrepancies between both pathways ranging from 10% to 50%.

Regarding tracheal aggregate deposition (*Figure 5B*) nano-scale particles ($d_{ae}$ <10 nm) again exhibit highest accumulation probabilities (0.5-6%), whereas larger particles are usually enabled to pass this proximal airway without any significant difficulties. Contrary to the extrathoracic region, particles inhaled through the mouth are characterized by higher deposition efficiencies than particles inspired through the nose. This particle transport behaviour is also given in a similar fashion in the following airway generations of the tracheobronchial tree, being characterized by partly asymmetric airway bifurcations. Additionally, in the main bronchi of airway generation 1 (*Figure 5C*) deposition of aggregates with $d_{ae}$ >10 nm is marked by increased relevance (>1%), whilst smaller particles show a slight decrease in deposition. This trend may be also observed for airway generations 2 to 4 (*Figure 5D,E,F*), whereby total numbers of deposited particles are generally subject to a decline with proceeding penetration of the lung airways. Comparison of nasal and oral inhalation shows that higher particle numbers are enabled to enter the lungs after passage of the oral pathway, whereas inhalation through the nose results in an enhanced capture of particles in the nasal airways.

For light-work breathing scenarios respective modelling results are summarized in the graphs of *Figure 6*. Basically, the deposition functions computed for nasal and oral inhalation on the one hand and different sites of the human respiratory tract on the other hand are rather similar to those introduced in *Figure 5*. Due to the higher velocity of the air stream during light-work inhalation nano-scale particles with $d_{ae}$ <10 nm are commonly subject to declined deposition probabilities in the single airways. Contrary to that, larger aggregates exhibit slightly higher deposition probabilities in the extrathoracic compartments and airways of the uppermost lungs. As illustrated in the respective graphs, relative deposition in the nasal/oral airways amounts to 32% to 100%, that in the trachea to 0.2% to 4.5%, whilst that in the remaining bronchial airways being of interest in this study varies between 0% and 4%.

Summing up the computation results presented above, aggregate deposition may be described as a function of (I) aggregate size; (II) deposition site; and (III) breathing conditions, whereby, under the frame conditions assumed for this study, highest particle doses are delivered to the

 

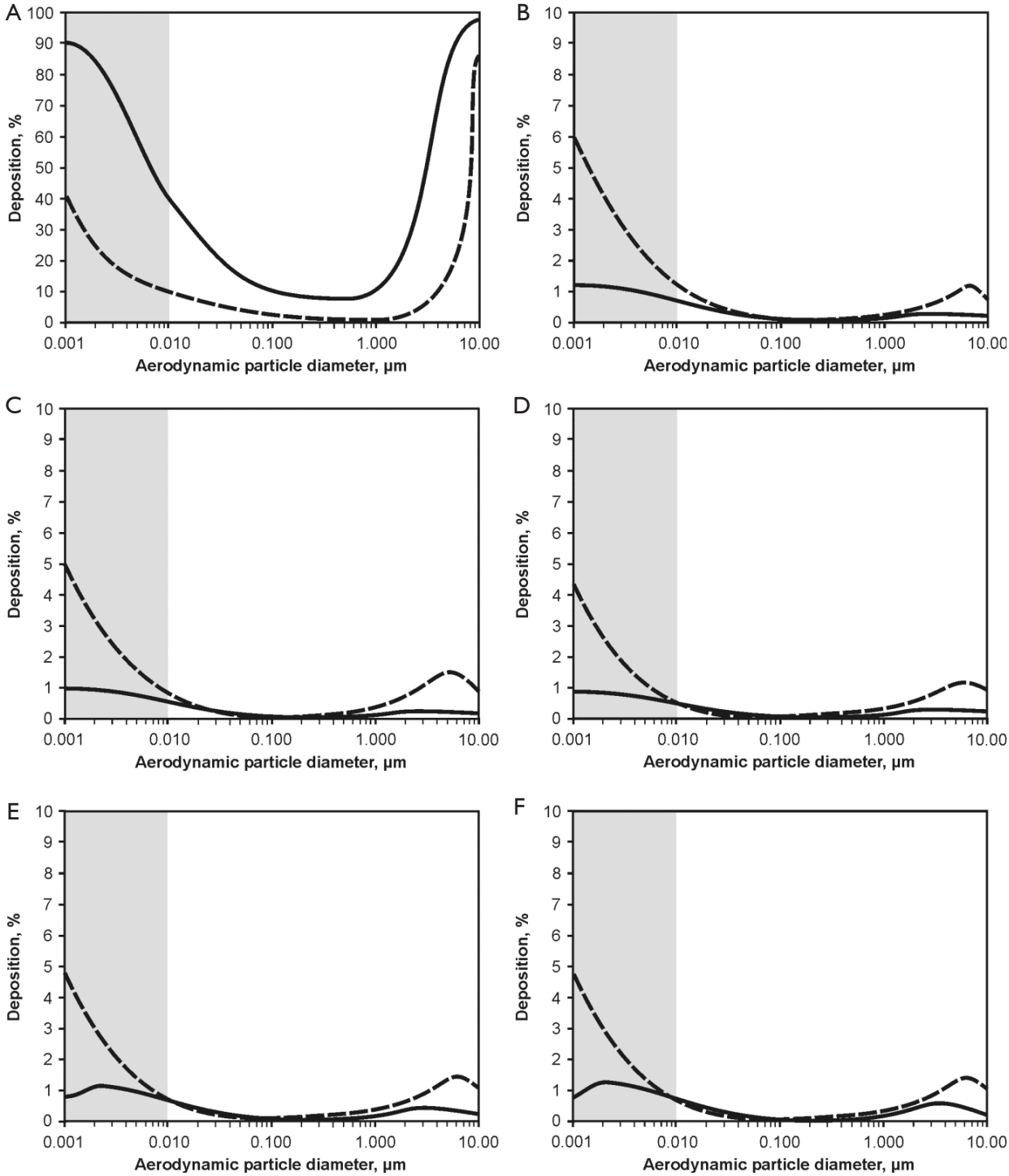


**Figure 5** Graphs illustrating the dependence of local aggregate deposition on aerodynamic diameter assuming sitting breathing conditions (28). A. Extrathoracic region; B. Trachea (lung generation 0); C. Main bronchi (lung generation 1); D. Lung generation 2; E. Lung generation 3; F. Lung generation 4. Solid lines mark deposition following oral inhalation, whereas dashed lines mark deposition after nasal inhalation

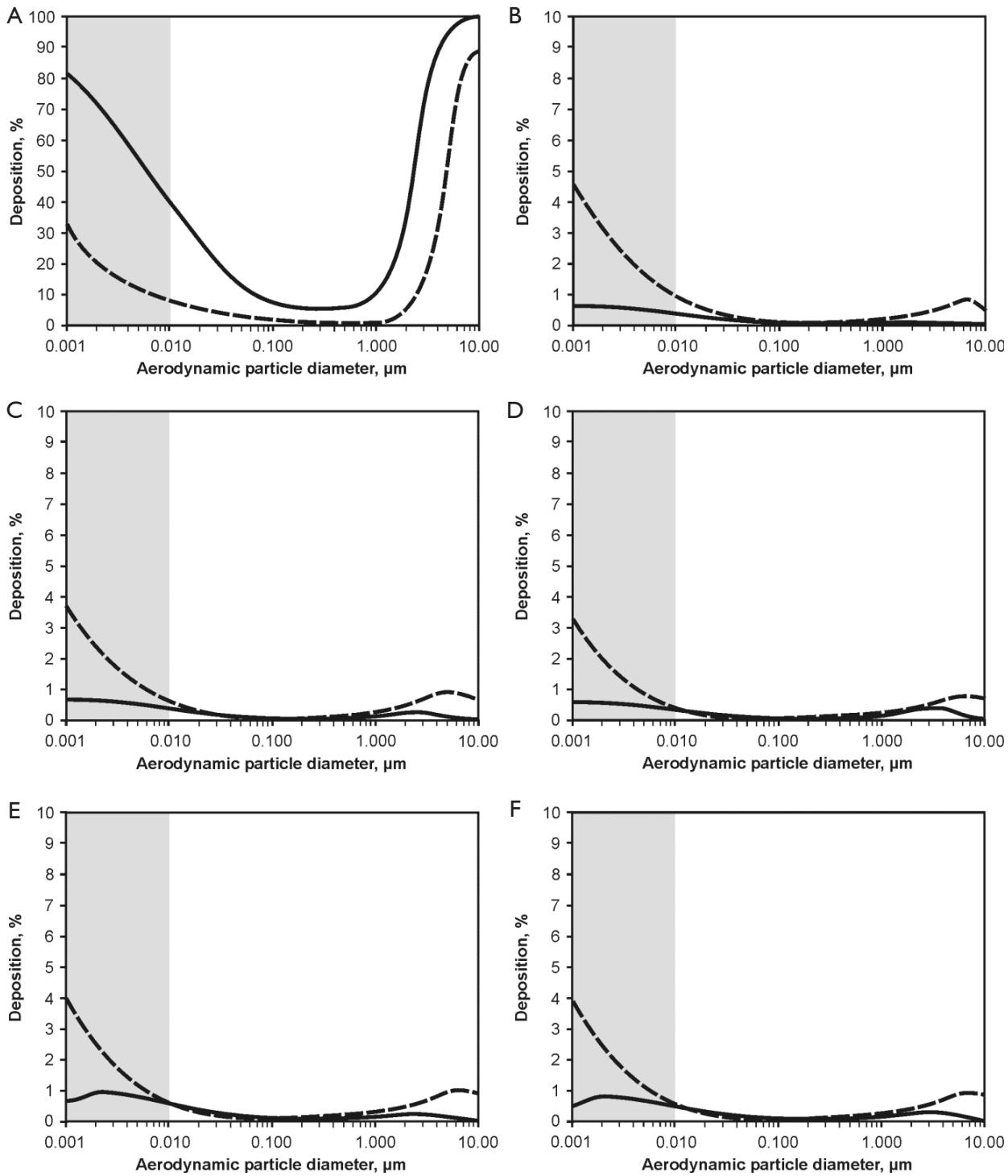


**Figure 6** Graphs illustrating the dependence of local aggregate deposition on aerodynamic diameter assuming light-work breathing conditions (28). A. Extrathoracic region; B. Trachea (lung generation 0); C. Main bronchi (lung generation 1); D. Lung generation 2; E. Lung generation 3; F. lung generation 4. Solid lines mark deposition following oral inhalation, whereas dashed lines mark deposition after nasal inhalation

 

extrathoracic regions, the trachea as well as the main bronchi.

## Discussion

Realistic evaluation of health hazards that emanate from the exposure to nano-scale aggregates requires comprehensive information regarding the behaviour of such highly complex particles in the human respiratory system. During the past two decades theoretical approaches to that problem were developed which meanwhile represent an appropriate support for any determination of aggregate deposition in the lung airways and its effects on the lung tissue (5-8,19). In this contribution, deposition of variably shaped aggregates was simulated by using two standard breathing conditions (sitting and light-work breathing) (28). The results obtained from the study may be regarded as helpful in several aspects: first, it could be demonstrated that aggregates with unit density (1.0 $g \cdot cm^{-3}$) are characterized by a lung deposition which in part differs significantly from that of comparable spheres, where all computed particle diameters (i.e., $d_{ev}$, $d_{es}$, and $d_{ae}$) take the same value. Second, deposition behaviour of aggregates is affected to a high extent by several physical factors that, among other, include aggregate shape and compactness (i.e., the occurrence of internal voids) (19,22,23). The second finding was already outlined in experimental studies, where rats were exposed to nano-scale particles of highly irregular shape (17,18).

Basically, deposition of nanoscale aggregates in the human respiratory system is determined by four deposition mechanisms, among which only Brownian diffusion has a significant effect, whilst inertial impaction, interception, and sedimentation are characterized by minor to negligible influences (20,28). As an essential consequence of this phenomenon aggregates with an aerodynamic diameter <10 nm are already filtered to a high extent in the extrathoracic airways, whereby deposition efficiency in the nasal pathway exceeds that in the oral pathway by a factor of 1.5 to 2.0. Aggregates ranging in size from 10 to 100 nm are marked by two properties: first, their total deposition in the human respiratory tract is significantly declined with respect to smaller particles; Second, their probability to penetrate to deeper lung regions is remarkably increased (32-35).

An interesting problem concerns the modification of aggregate deposition with increasing tidal volume and inhalative flow rate. As could be already demonstrated for ideal spherical particles, any enhancement of both the breathing frequency and the tidal volume has two major effects: first, inertial impaction and interception of larger particles ($d_{ae}$ >100 nm) are significantly increased, causing a deposition concentration of these particles in the uppermost parts of the human respiratory tract. Second, Brownian diffusion mostly affecting nanoscale particles is subject to a noticeable dislocation to more distal regions of the pulmonary system (21-24). As demonstrated in *Figures 5*,*6*, these essential findings obtained for spheres may be also transferred to irregularly shaped particle aggregates.

This contribution confirms the widely accepted paradigm, according to which biopersistent aggregates may represent remarkable health hazards (36-39). Results of the comprehensive computations clearly show that under breathing conditions resulting from physical strain smallest aggregates ($d_{ae}$ <10 nm) have an enhanced ability to penetrate to the upper bronchi and even deeper parts of the lungs (i.e., the respiratory bronchioli and alveoli), where they are subject to different clearance processes (23). A certain fraction is stored in the lung parenchyma, where it may induce numerous lung diseases and, in the worst case, may act as severe carcinogen. Under conditions of rather slow inhalation (e.g., sitting breathing) nano-scale aggregates ($d_{ae}$ <10 nm), on the other hand, are almost completely filtered in the uppermost parts of the human respiratory system, where most of them are cleared by fast clearance mechanisms such as the mucociliary escalator (28). Nevertheless, also bronchial sites with increased accumulation of carcinogenic material (i.e., the carinal ridges of bronchial bifurcations) may be affected by pathological modifications, at the end of which stands the formation of various malign tumours (*Figure 7*) (36-39).

From the results provided in this study it may be concluded that nanoscale particle aggregates may become serious health hazards and, in the worst case, also triggers of malign transformation. This circumstance depends upon the (I) effective size of the aggregates and (II) the intensity of particle inhalation. Although particle deposition scenarios are simulated with high accuracy in the meantime, further refinements of respective deposition models have to be done in near future.

 

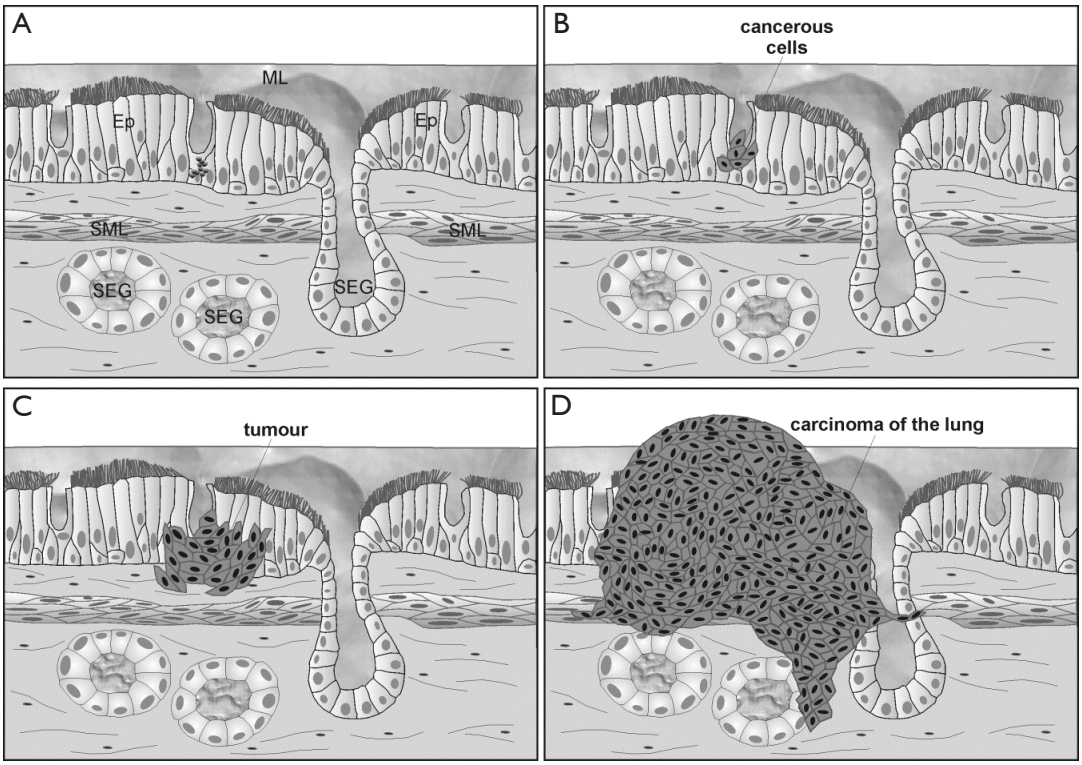


**Figure 7** Single stages of carcinogenesis in the extrathoracic/bronchial epithelium. A. Particle deposition and take up; B. Formation of cancerous cells; C. Development of a tumour; D. Final carcinoma formation. Abbreviations: Ep, epithelium; ML, mucus layer; SEG, subepithelial gland; SML, smooth muscle layer

## Acknowledgements

*Disclosure:* The author declares no conflict of interest.

## References

1. Baron PA, Mazumder MK, Cheng YS. Direct-reading techniques using particle motion and optical detection. In: Baron PA, Willeke K. eds. Aerosol measurement: principles, techniques, and applications. New York: John Wiley, 2001:705-49.
2. Flagan RC. Electrical techniques. In: Baron PA, Willeke K. eds. Aerosol measurement: principles, techniques, and applications. New York: John Wiley, 2001:537-68.
3. Sturm R. Theoretical and experimental approaches to the deposition and clearance of ultrafine carcinogens in the human respiratory tract. Thoracic Cancer 2011;2:61-8.
4. Wexler AS, Johnston MV. Real-time single-particle analysis. In: Baron PA, Willeke K. eds. Aerosol measurement: principles, techniques, and applications. New York: John Wiley, 2001:365-86.
5. Kasper G. Dynamics and measurement of smokes. I Size characterization of nonspherical particles. Aerosol Sci Technol 1982;1:187-99.
6. Stöber W. Dynamic shape factors of nonspherical aerosol particles. In: Mercer T. ed. Assessment of airborne particles. Springfield: Charles C. Thomas, 1972:249-89.
7. Dahneke BE. Slip correction factors for nonspherical bodies—I Introduction and continuum flow. J Aerosol Sci 1973;4:139-45.
8. Dahneke BE. Slip correction factors for nonspherical bodies—II Free molecular flow. J Aerosol Sci 1973;4:147-61.
9. Davies CN. Particle-fluid interaction. J Aerosol Sci 1979;10:477-513.
10. DeCarlo PF, Slowik JG, Worsnop DR, et al. Particle morphology and density characterization by combined mobility and aerodynamic diameter measurements. Part 1: theory. Aerosol Sci Technol 2004;38:1185-205.
11. Katrinak KA, Rez P, Perkes PR, et al. Fractal geometry of carbonaceous aggregates from an urban aerosol. Environ Sci Technol 1993;27:539-47.

 

12. Bayram H, Ito K, Issa R, et al. Regulation of human lung epithelial cell numbers by diesel exhaust particles. Eur Respir J 2006;27:705-13.
13. Bayram H, Devalia JL, Sapsford RJ, et al. The effect of diesel exhaust particles on cell function and release of inflammatory mediators from human bronchial epithelial cells in vitro. Am J Respir Cell Mol Biol 1998;18:441-8.
14. Kasper G. Dynamics and measurement of smokes. 2. The aerodynamic diameter of chain aggregates in the transition regime. Aerosol Sci Technol 1982;1:201-15.
15. Rogak SN, Flagan RC, Nguyen HV. The mobility and structure of aerosol agglomerates. Aerosol Sci Technol 1993;18:25-47.
16. Slowik JG, Stainken K, Davidovits P, et al. Particle morphology and density charcterization by combined mobility and aerodynamic diameter measurements. Part 2: application to combustion generated soot particles as a function of fuel equivalence ratio. Aerosol Sci Technol 2004;38:1206-22.
17. Brain JD. Animal studies with environmental aerosols. J Aerosol Med 1993;6:33-7.
18. Mauderly JL, Gillett NA, Henderson RF, et al. Relationships of lung structural and functional changes to accumulation of diesel exhaust particles. Ann Occup Hyg 1988;32:659-69.
19. Sturm R. Theoretical models for dynamic shape factors and lung deposition of small particle aggregates originating from combustion processes. Z Med Phys 2010;20:226-34.
20. Koblinger L, Hofmann W. Monte Carlo modeling of aerosol deposition in human lungs. Part I: simulation of particle transport in a stochastic lung structure. J Aerosol Sci 1990;21:661-74.
21. Sturm R, Hofmann W. Stochastic model for the spatial visualization of particle-deposition patterns in the lung and their significance in lung medicine. Z Med Phys 2006;16:140-7.
22. Sturm R, Hofmann W. A computer program for the simulation of fiber deposition in the human respiratory tract. Comput Biol Med 2006;36:1252-67.
23. Sturm R, Hofmann W. A theoretical approach to the deposition and clearance of fibers with variable size in the human respiratory tract. J Hazard Mater 2009;170:210-8.
24. Sturm R. Deposition and cellular interaction of cancer-inducing particles in the human respiratory tract: theoretical approaches and experimental data. Thoracic Cancer 2010;4:141-52.
25. Koblinger L, Hofmann W. Analysis of human lung morphometric data for stochastic aerosol deposition calculations. Phys Med Biol 1985;30:541-56.
26. Raabe OG, Yeh HC, Schum GM, et al. Tracheobronchial geometry: human, dog, rat, hamster—a compilation of selected data from the project respiratory tract deposition models. Albuquerque: Lovelace Foundation, 1976.
27. Haefeli-Bleuer B, Weibel ER. Morphometry of the human pulmonary acinus. Anat Rec 1988;220:401-14.
28. International Commission on Radiological Protection (ICRP): Human respiratory tract model for radiological protection, Publication 66. Oxford: Pergamon Press,1994.
29. Hofmann W, Koblinger L. Monte Carlo modeling of aerosol deposition in human lungs. Part II: deposition fractions and their sensitivity to parameter variations. J Aerosol Sci 1990;21:675-88.
30. Shi H, Kleinstreuer C, Zhang Z. Modeling of inertial particle transport and deposition in human nasal cavities with wall roughness. J Aerosol Sci 2007;38:398-419.
31. Sandeau J, Katz I, Fodil R, et al. CFD simulation of particle deposition in a reconstructed human oral extrathoracic airway for air and helium-oxygen mixtures. J Aerosol Sci 2010;41:281-94.
32. Cheng YS, Zhou Y, Chen BT. Particle deposition in a cast of human oral airways. Aerosol Sci Technol 1999;31:286-300.
33. Cheng YS. Aerosol deposition in the extrathoracic region. Aerosol Sci Technol 2003;37:659-71.
34. Albuquerque PC, Gomes JF, Bordado JC. Assessment of exposure to airborne ultrafine particles in the urban environment of Lisbon, Portugal. J Air Waste Manag Assoc 2012;62:373-80.
35. Gomes JF, Albuquerque PC, Miranda RM, et al. Determination of airborne nanoparticles from welding operations. J Toxicol Environ Health A 2012;75:747-55.
36. IARC working group on the evaluation of carcinogenic risks to humans. Man-made vitreous fibres. IARC Monogr Eval Carcinog Risks Hum 2002;81:1-381.
37. Muscat JE, Wynder EL. Cigarette smoking, asbestos exposure, and malignant mesothelioma. Cancer Res 1991;51:2263-7.
38. Bianchi C, Bianchi T. Malignant mesothelioma: global incidence and relationship with asbestos. Ind Health 2007;45:379-87.
39. Travis WD, Travis LB, Devesa SS. Lung cancer. Cancer 1995;75:191-202.

**Cite this article as:** Sturm R. Theoretical deposition of carcinogenic particle aggregates in the upper respiratory tract. Ann Transl Med 2013;1(3):25. doi: 10.3978/j.issn.2305-5839.2013.07.06

 